

Short Communication

Effect of deposition of Al/AlN coating on medium-Mn steel on its corrosion resistance in 5 wt.% NaCl

Hongru Yang¹, Xiaoyan Liu^{1,2,*}, Xiliang Zhang^{1,*}, Changsheng Wu¹, Yanqin Wang¹, Xiaosong Zhu¹, Yuan Zhang¹, Zhiwei Zhao¹

¹ School of Materials Science and Engineering, Hebei University of Engineering, Handan 056038, Hebei, China

² Hebei Engineering Research Centre for Rare Earth Permanent Magnetic Materials & Applications, Hebei University of Engineering, Handan 056038, Hebei, China

*E-mail: x918y@126.com; xlzhang@hebeu.edu.cn

Received: 27 May 2022 / Accepted: 29 July 2022 / Published: 17 November 2022

Medium-Mn steel has wide use in marine structures because of its low alloy cost, high strength, and high toughness. However, it has poor corrosion resistance in the marine atmosphere. In this paper, Al/AlN double-layer coating was fabricated on medium-Mn steel to improve its corrosion resistance. An Al/AlN double-layer was deposited on the surface of medium-Mn steel by direct current magnetron sputtering. The effect of Al/AlN film deposition on the corrosion behavior of medium-Mn steel was investigated by X-ray diffraction, scanning electron microscopy, and electrochemistry. The corrosion environment is the marine atmosphere, which is simulated using the neutral salt spray test. The results showed that AlN and Al can provide excellent protection against corrosion for medium-Mn steel. Medium-Mn steel coated with Al/AlN double films has high rust layer density after corrosion, and the corrosion products contain more anti-corrosion phase α -FeOOH. The deposition of Al/AlN thin films can restrain the formation of Mn_xO_y . The corrosion current density decreases from 2.389×10^{-4} to $3.718 \times 10^{-5} \text{ A} \cdot \text{cm}^{-2}$. The deposition of Al/AlN double-layer films can effectively improve the corrosion resistance of medium-Mn steel in the marine atmosphere.

Keywords: DC magnetron sputtering, Medium-Mn steel, Corrosion resistance, Marine atmosphere

1. INTRODUCTION

Medium-Mn steel has wide use in marine structures, ship plates, and bridges because of its low alloy cost, high strength, and high toughness [1]. It has great potential to replace the traditional offshore platform rack steel Q690 [2,3]. Nevertheless, medium-Mn steel typically contains fewer corrosion-resistance elements, such as Mo [4] and Ni [5]. Meanwhile, Mn has adverse an effect on corrosion resistance [6]. This results in poor corrosion resistance of medium-Mn steel in the marine atmosphere

and can reduce its service life on the offshore platform. Therefore, it is crucial to improve the corrosion resistance of medium-Mn steel.

Besides the addition of corrosion-resistance elements to the matrix [7], surface modification is an efficient method for improving the resistance of the steel [8]. Yufen Zhang coated 65-mn steel with a hydrophobic coating of calcium stearate with a layered micro/nanostructure by direct current (DC) electrodeposition and demonstrated the steel's good corrosion resistance [9]. Mian Wu demonstrated that the HVOFNi60 coating not only has good corrosion resistance but also excellent wear resistance [10]. Magnetron sputtering technology is a common physical vapor deposition method for preparing surface coating, and it is environmentally friendly [11]. The thickness of the surface coating and the grain size can be controlled precisely by adjusting magnetron sputtering parameters [12,13].

AlN ceramics have been widely used because of their excellent mechanical properties, sufficiently high-temperature compatibility [11], and excellent corrosion resistance [14]. They have been widely used in coating the surfaces of Al, Mg, and other metals [15]. Few reports have mentioned the effects of AlN ceramics surface coating on the corrosion behavior of medium-Mn steel. Therefore, AlN ceramics are chosen as the surface coating for medium-Mn steel in this work, and magnetron sputtering technology is applied.

The marine environment is divided into five different areas in the vertical direction according to the differences in moisture, temperature, and oxygen content, the ocean-atmosphere area, the ocean splash area, the sea tidal range, the seawater full immersion area, and the submarine mud area [16-18]. Different types and degrees of corrosion will occur in each area according to its conditions. In areas above sea level, electrochemical corrosion is dominant because of the high content of salt and moisture. The ocean-atmosphere zone above the mean ocean tide line is the severe electrochemical corrosion zone, which erodes severely steels [19].

Because the voltage of Al is lower than that of Fe and correspondingly, it works as the anode during the electrochemical process and can protect the matrix. As a result, Al is chosen as a buffer layer, and the working layer of AlN was deposited on the medium-Mn steel by DC magnetron sputtering technology in this work. The neutral salt spray test was used to simulate the corrosion environment of the marine atmosphere zone, and the corrosion test was conducted using medium-Mn steel with and without surface coating. The influence of the surface coating on the corrosion behavior of medium-Mn steel was explored. The mechanism was investigated by surface morphology, composition analysis, and electrochemical corrosion performance.

2. EXPERIMENT

2.1 Material preparation

A 50-kg ingot of Fe-8.26Mn-0.2C-1.71Al (wt.%) steel was melted using a vacuum induction furnace and then forged into 30-mm-thick slabs. The specific ingredients are listed in Table 1. After homogenization treatment at 1200°C for 2 h, the slabs were hot-rolled (HR) to 4 mm at 850°C and then cooled to room temperature. Inter-critical annealing (IA) at 680°C for 1 h for the HR sheet was

performed before cold rolling (CR) to a thickness reduction of 45%. Subsequently, the CR sheet was annealed at 680°C for 10 min, followed by cooling in air.

Table 1. Medium-Mn steel composition in the experiment

Samples	C	Mn	Al	Fe
In mass (%)	0.2	8.26	1.71	89.83

2.2 Coating deposition

Al/AlN double-layer films were deposited on the specimens by DC magnetron sputtering. The magnetron sputtering system was JC-500M3 manufactured by Beijing Techno Technology Co., Ltd. Aluminum with a purity level of 99.99% was used as a target. The medium-Mn steels were all polished and then ultrasonically cleaned in alcohol and acetone for 15 min before surface coating. Al/AlN double-layer films were deposited in two steps. The Al film was deposited in an argon atmosphere, and then AlN was deposited in N₂-Ar mixed atmosphere with a flow ratio of 0.5. The two films were deposited for 90 min with a target power of 300 W and a working pressure of 0.5 Pa. The preparation process parameters of the films are listed in Table 2.

Table 2. Process parameters for the preparation of Al/AlN bilayer films by magnetron sputtering

	Pressure control (Pa)	Power (W)	N ₂ /Ar (sccm)	Deposition time (min)
Al	0.5	300	0:40	90
AlN	0.5	300	20:40	90

2.3 Neutral salt spray test

The corrosion behavior was characterized by the neutral salt spray test at 35°C, simulating the corrosion environment of the marine atmosphere zone. The corrosion solution was 5-wt.% NaCl with a pH value of 6.5–7.2. The average sedimentation rate of the horizontal area of 80 cm² was 1.5 mL/h ± 0.5 mL/h. The corrosion durations were 12, 24, 48, 72, 96, and 144 h. After corrosion exposure for different durations, the samples were analyzed by X-ray diffraction (XRD), scanning electron microscopy (SEM), and electrochemistry. The scanning electron microscope was an ULTRA 55 field emission electron microscope manufactured by ZEISS. The system used in electrochemistry was Shanghai Chenhua CHI600E series electrochemical workstation.

2.4 Electrochemical tests

The electrochemical test was conducted using the CHI600E electrochemical workstation, using a three-electrode system. The electrolytic solution was 5-wt.% NaCl. The potential range was between -1.5 and 0.5 V with a scanning rate of 1 mV/s.

2.5 Microscopic morphology and composition analysis

The morphology observation of the rust layer was performed using an Ultra 55 field emission scanning electron microscope manufactured by ZEISS. The samples were sprayed with gold on their steel surfaces. The composition of the corrosion products was analyzed using a DMAX-2500/pc X-ray diffractometer with Cu K-alpha radiation at a scan rate of 4°/min. The wavelength of the X-ray was 0.154178 nm.

3. RESULTS AND DISCUSSION

3.1 Thin film phase analysis

Fig. 1 shows the XRD diffraction pattern of the coated medium-Mn steel. Al and AlN are abundant, implying that the deposition is of high quality. Only Fe can be detected in the medium-Mn steel. This may be due to the highly preferred orientation growth of Al and AlN, so the signal of other phases with low content cannot be detected.

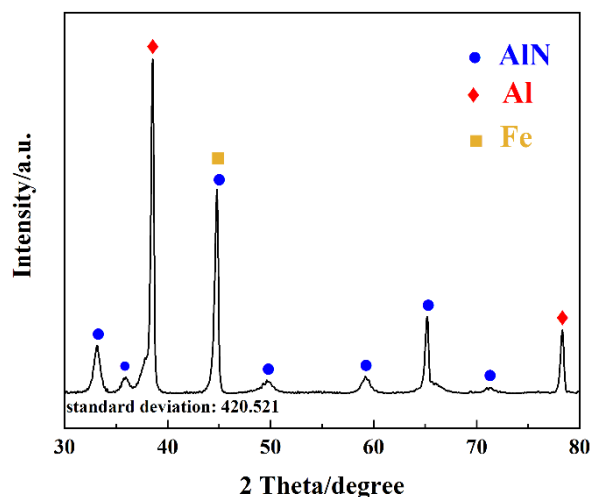


Figure 1. XRD diffraction pattern of medium-Mn steel surface after deposition of Al/AlN films

3.2 Corrosion product phase analysis

Fig. 2a and Fig. 2b show the XRD patterns of the corrosion products of the coated and uncoated medium-Mn steel after corrosion exposure for different durations. After corrosion exposure for 12 h, there is a high content of Fe in the uncoated sample (Fig. 2a), implying that the surface had not been completely covered by the rust layer. α -FeOOH is barely detected at this stage; meanwhile, Fe_3O_4 , Fe_2O_3 , γ -FeOOH, and Mn_xO_y are abundant, and the content of $(\text{Fe}, \text{Mn})_x\text{O}_y$ is low. With increasing corrosion time, the content of γ -FeOOH and Mn_xO_y decreases, whereas that of α -FeOOH and $(\text{Fe}, \text{Mn})_x\text{O}_y$ increases slightly.

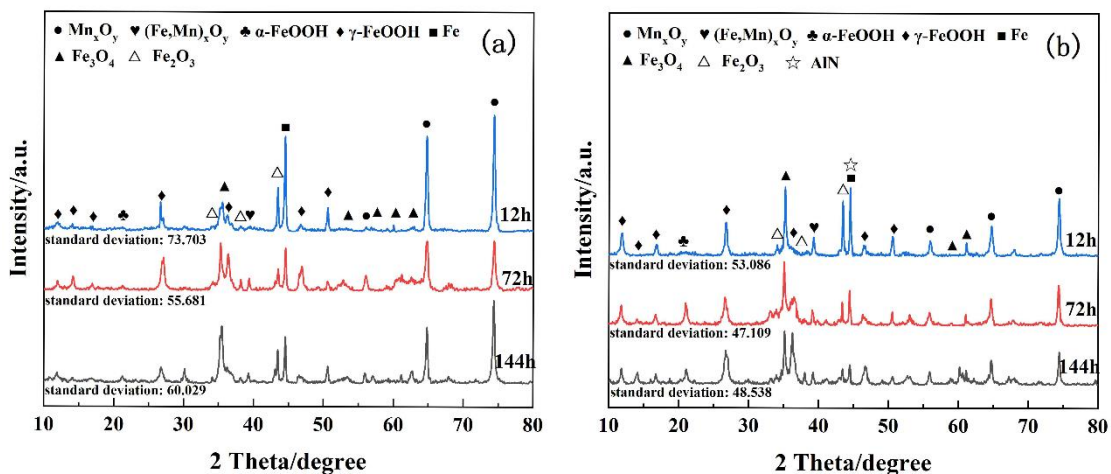


Figure 2. XRD diffraction patterns of corrosion products after salt spray corrosion for 12, 72, and 144 h. (a) Uncoated medium-Mn steel; (b) Coated medium-Mn steel

Different phenomena appear in the coated medium-Mn steel after corrosion for different durations. After corrosion exposure for 12 h (Fig. 2b), although the content of Fe₃O₄, Fe₂O₃, and γ-FeOOH in the rust layer of the coated medium-Mn steel slightly increases compared with that of the uncoated one, the content of Mn_xO_y decreases rapidly. AlN can be detected in the rust layer, whose peak coincides with that of pure Fe at approximately 44°. This means that the surface of the medium-Mn steel has not been covered with the corrosion rust layer. With an increase in duration, the surface of the sample is completely covered with the corrosion rust layer, and AlN cannot be detected. The signal of Fe₃O₄, Fe₂O₃, and γ-FeOOH decreases, whereas that of α-FeOOH increases. After corrosion exposure for 72 and 144 h, the signal of α-FeOOH is higher in Fig. 2b than in Fig. 2a.

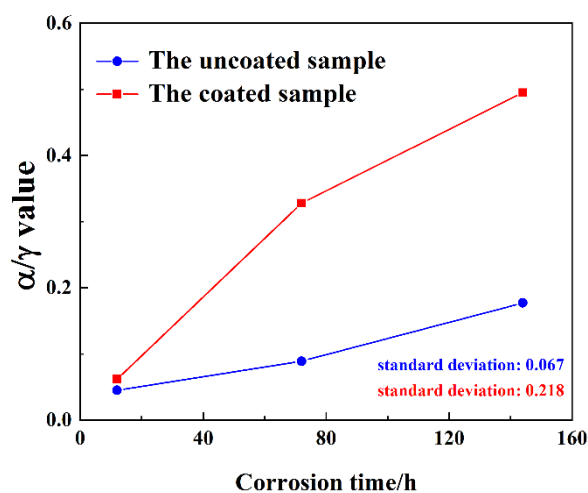


Figure 3. α / γ values of two samples after salt spray corrosion for 12, 72, and 144 h

The value of α/γ (means α-FeOOH to γ-FeOOH) is given in Fig. 3. The α/γ value of the uncoated sample is only 0.045, and that of the coated one is slightly higher. With increasing corrosion duration, the values of the two uncoated samples increase slightly, whereas that of the coated sample increases

significantly. After corrosion exposure for 144 h, the α/γ value of the coated medium-Mn steel increases to 0.495, approximately 2.8 times as large as that of the uncoated steel.

3.3 Macroscopic morphology of corrosion product surface

Fig. 4a.b.c show the macromorphology of the rust layer of the uncoated medium-Mn steel after corrosion for various durations. At the initial stage of corrosion, the rust layer formed on the surface of the sample is thin, and it does not completely cover the surface of the sample (Fig. 4a). The substrate is exposed to a corrosive environment, and the rust layer cannot protect the medium-Mn steel. The corrosion product is bright yellow at this stage, and it is mainly composed of low-valent iron oxides (Fig. 2a). After 72-h corrosion exposure, corrosion proceeds violently. The thickness of the rust layer is significantly increased, and the surface of the sample is covered uniformly (Fig. 4b). The color of the rust layer gradually changes to brown, and there is still a part of the black rust layer. This is because the oxides of low-valent iron ions have gradually transformed into Fe_3O_4 . In Fig. 4c, when the corrosion time reaches 144 h, the overall corrosion process has entered a stable state. The rust layer is very dense and thick, and it has completely covered the surface of the sample.

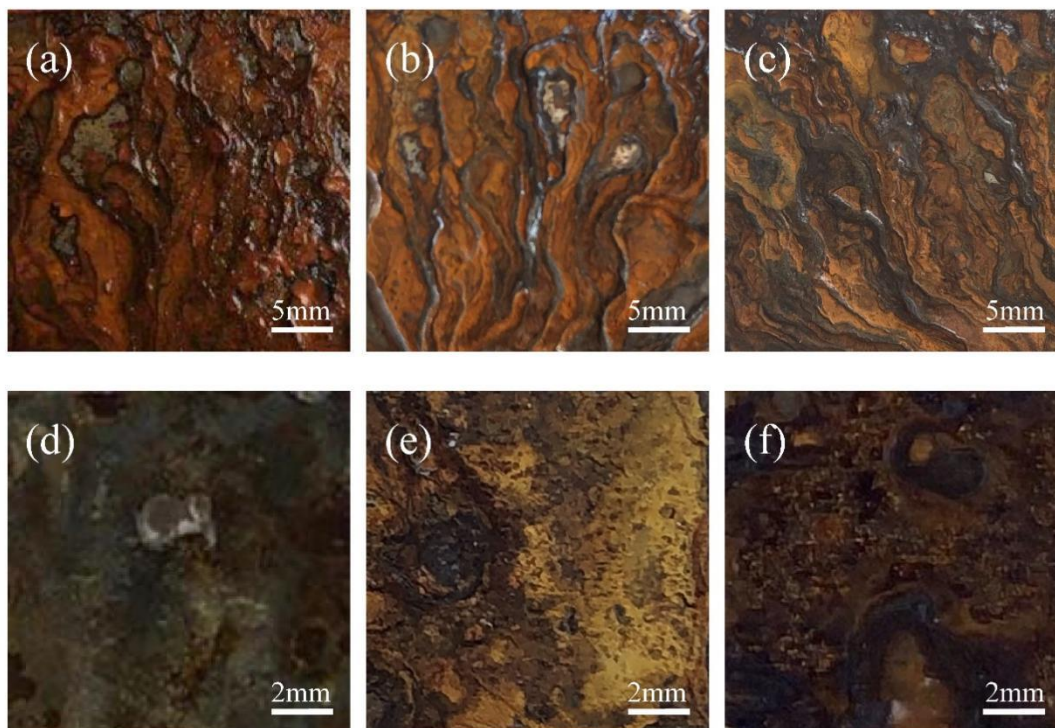


Figure 4. Macroscopic surface morphology of rust layer after salt spray corrosion for various durations Uncoated medium-Mn steel (a) 12 h, (b) 72 h, and (c) 144 h Coated medium-Mn steel (d) 12 h, (e) 72 h, and (f) 144 h

At this stage, the rust layer completely isolates the substrate from the corrosive liquid, and it plays a role in protecting the substrate. The overall color of the corrosion products turns dark brown, and a large amount of rust layer appeared black. This is because more phases are transformed into Fe_3O_4 .

Figs. 4d.e.f show the macromorphology of the rust layer of the coated medium-Mn steel after corrosion exposure for various durations. After 12-h corrosion exposure, only a small amount of corrosion product is observed on the surface of the sample, and the rust layer does not appear continuously (Fig. 4d). The color of the substrate remained dark blue, which is the color of the Al/AlN film. This indicates that the corrosion rate of the coated sample is significantly lower than that of the uncoated one. When the corrosion exposure time reaches 72 h, a thin layer of rust forms but does not cover the entire matrix. With an increase in duration up to 144 h, a dark continuous rust layer forms on the surface of the sample, covering the entire surface of the substrate. However, the thickness of the rust layer is small, and no heavy corrosion products had been generated. The overall color of the rust layer is dark brown. Based on the XRD analysis results, most of the rust layer products are converted to Fe_3O_4 .

Compared with Figs. 4a.b.c and 4d.e.f, the formation rate of corrosion products on the surface of the coated sample is significantly reduced after the same corrosion duration, and the thickness of the rust layer is significantly reduced. Therefore, the coating of Al/AlN film has a remarkable protective effect on the medium-Mn steel.

3.4 Microscopic morphology of corrosion products

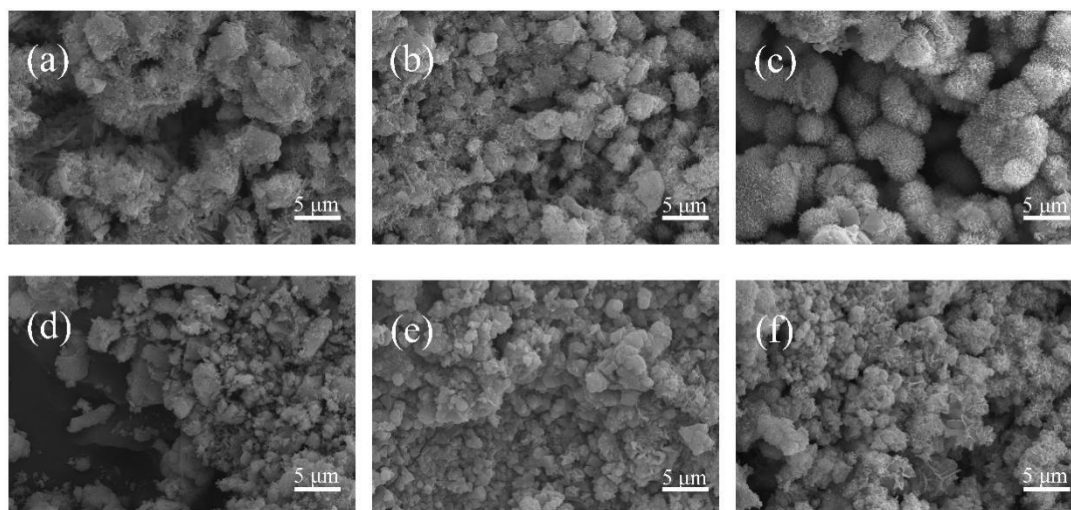


Figure 5. Microscopic surface morphology of rust layer after salt spray corrosion for various durations Uncoated medium-Mn steel (a) 12 h (b) 72 h (c) 144 h Coated medium-Mn steel (d) 12 h (e) 72 h (f) 144 h

Figs. 5a.b.c and 5d.e.f show SEM images of the corrosion products of the sample with and without surface coating. After 12-h corrosion exposure (Figs. 5a and 5d), the corrosion products mainly have a flake structure, which is a typical structure of $\gamma\text{-FeOOH}$. At this stage, the overall structure of the rust layer is loose and porous, and the rust layer does not cover the entire surface of the sample. Due to

the protection of the Al/AlN film, the medium-Mn steel is corroded slightly in Fig. 5d, and the rust layer is very thin.

After 72-h corrosion exposure, the rust layer covered the entire surface of the uncoated sample (Fig. 5b). There are many pores in the corrosion product. This structure can provide channels for the corrosive liquid and increase the corrosion rate. Compared with Fig. 5b, the corrosion product in Fig. 5e is small and compact, providing better protection to the matrix. When the corrosion exposure duration reaches 144 h, the density of the rust layer of the two samples is significantly improved, and the overall corrosion resistance of the samples is improved. “Whisker”-like attachments appear on the surface of the corrosion products both in Fig. 5c and Fig. 5f. This is a typical structure of α -FeOOH and makes the rust layer more compact. α -FeOOH plays a role in improving the corrosion resistance of materials and reducing the corrosion rate. The corrosion product of the coated medium-Mn steel is small, and the rust layer is significantly denser than that of the uncoated one.

Fig. 6 shows the morphology of the cross-section of the uncoated and coated medium-Mn steels. The corrosion production of the uncoated sample is approximately 212 μm , and it is loose and porous (The standard deviation is 5 μm). Coated with Al/AlN, the thickness of the corrosion production of the sample decreases significantly, and it is only approximately 70 μm (The standard deviation is 3 μm).

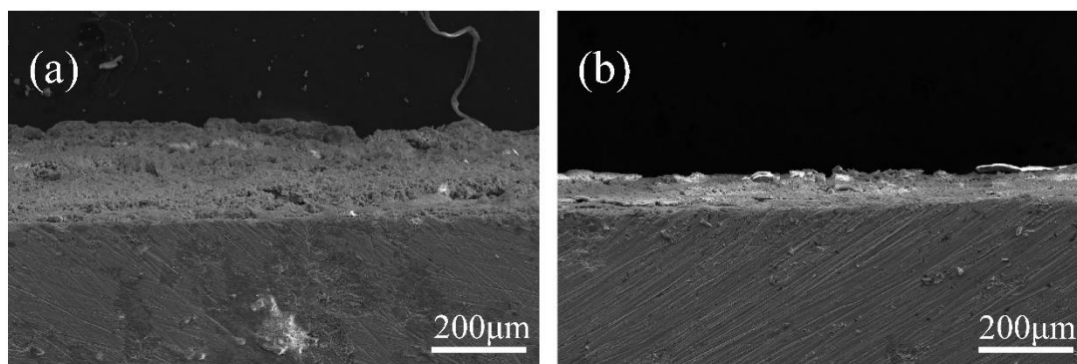


Figure 6. SEM image of rust layer cross-section of medium-Mn steel before and after coating after 144 h of salt spray corrosion (a) Uncoated medium-Mn steel (b) Coated medium-Mn steel

Fig. 7 shows the element distribution of the rust layer of the two samples after corrosion exposure for 144 h. Fig. 7a shows that there is no significant enrichment of elements in the rust layer of the uncoated sample. There are large amounts of Fe and O elements, and only a small amount of Al can be detected. The distribution of Mn is almost the same in both the rust layer and the matrix in Fig. 7a. When coated with the Al/AlN film, besides some enrichment in corrosion production (circled in Fig. 7b), the content of Mn is significantly lower in the rust layer than in the matrix. Al is significantly enriched in the middle of the corrosion production and near the interface between the coated film and the matrix. The enrichment of Fe near the interface is obvious in Fig. 7b.

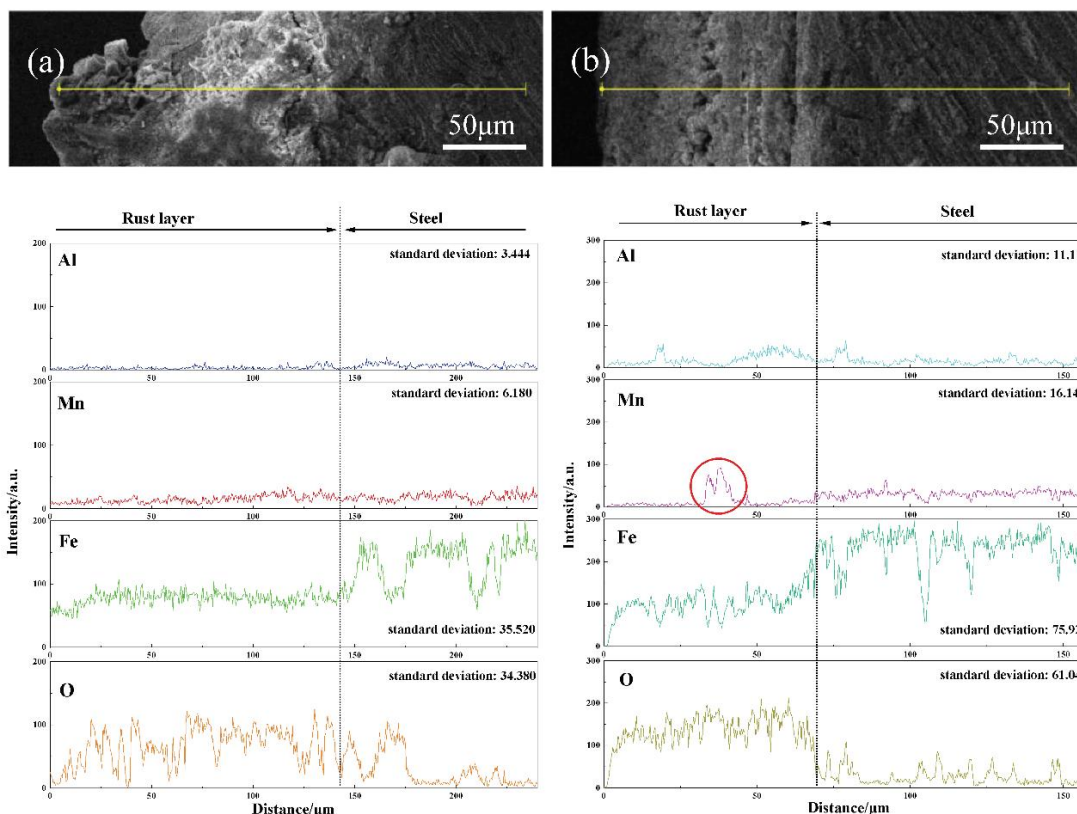


Figure 7. Elemental distribution of rust layer cross-section of two samples after salt spray corrosion for 144 h (a) Uncoated medium-Mn steel; (b) Coated medium-Mn steel

3.5 Electrochemical tests

Fig. 8 shows a comparison of the polarization curves of the coated and uncoated medium-Mn steels. The specific values of the corrosion potential and corrosion current density are shown in Table 3. The polarization curves of the two samples had similar variation trends, and no passivation occurs.

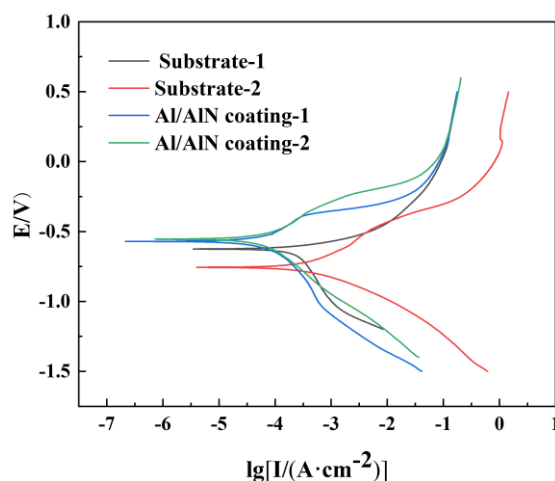


Figure 8. Polarization curves of coated medium-Mn steel and uncoated medium-Mn steel in 5-wt.% NaCl solution

Table 3. Electrochemical parameters of the four samples in 5 wt.% NaCl solution

Samples	E _{corr} (V)	I _{corr} (A·cm ⁻²)	Open circuit potential(V)
Substrate-1	-0.627	2.389×10 ⁻⁴	-0.654
Substrate-2	-0.756	2.708×10 ⁻⁴	-0.647
Al/AlN coating-1	-0.571	3.718×10 ⁻⁵	-0.595
Al/AlN coating-2	-0.555	3.992×10 ⁻⁵	-0.632

Fig. 8 shows that the corrosion potential is increased compared with that of the uncoated one, which means that the corrosion activity of the coated sample decreases. Meanwhile, the corrosion current density decreases by an order of magnitude, implying the lower corrosion rate of the coated medium-Mn steel. The results indicate that the corrosion resistance of the medium-Mn steel is significantly increased by the deposition of Al/AlN film.

4. DISCUSSION

The results of the corrosion test and macro and microanalyses indicate that medium-Mn steel is sensitive to the marine atmosphere, and the deposition of Al/AlN film can significantly improve the corrosion resistance of medium-Mn steel.

In this research, the corrosion products of medium-Mn steel in the marine atmosphere are mainly composed of Fe₃O₄, Fe₂O₃, α-FeOOH, γ-FeOOH, and (Fe, Mn)_xO_y (Fig. 2). Mn_xO_y is also detected in the medium-Mn steel, which is different from the corrosion products of general low-C steel. As reported in Ref [20], Mn_xO_y has a pore structure, which can provide channels for the corrosive liquid to contact the substrate. Therefore, Mn is averse to the corrosion resistance of medium-Mn steel, and the higher the content of Mn_xO_y, the lower the corrosion resistance of the steel. Fig. 2 shows that the content of Mn_xO_y is significantly lower in the coated medium-Mn steel than in the uncoated one. This indicated that the coating of Al/AlN can restrain the formation of Mn_xO_y and improve the corrosion resistance of medium-Mn steel.

Electrochemical corrosion is the main form of medium-Mn steel corrosion in the marine atmosphere, and Fe is easily oxidized to Fe²⁺. With sufficient oxygen, Fe²⁺ transforms into Fe(OH)₂ or FeOH⁺, and then γ-FeOOH. γ-FeOOH is unstable and has strong electrochemical activity, which negatively affects the protection of the matrix. In a high Cl⁻ environment, some γ-FeOOH transforms into β-FeOOH, and then α-FeOOH. α-FeOOH is the most stable iron oxyhydroxide [21]. It has the structure of a whisker, which can make the rust layer more compact, and it works as a barrier to isolate the corrosive liquid. Therefore, the corrosion resistance of medium-Mn steel greatly depends on the ratio of α-FeOOH and other iron oxides [22]. Typically, the larger the value of α/γ, the better the corrosion resistance of the material. The α/γ value of the coated medium-Mn steel is higher than that of the uncoated one during the corrosion process, and the longer the corrosion exposure duration, the greater the difference (Fig. 3). This also confirms that the deposition of Al/AlN can improve the corrosion resistance of medium-Mn steel.

From the corrosion morphology and the electrochemical analysis, we can conclude that the deposition of Al/AlN film can improve the corrosion resistance of medium-Mn steel in this study. Compared with previous research [23], cracks in the corrosion products can be observed in the medium-Mn steel after corrosion exposure for 72 h, whereas there is no obvious crack in the coated medium-Mn steel in this work.

The AlN ceramic film has excellent stability and corrosion resistance property. The Al thin film has two functions in this work. First, it is a buffer layer to improve the adhesion between AlN and the matrix. Second, it works as the anode during the electrochemical process because the voltage of Al is lower than that of Fe; it can also protect the matrix.

Fig. 9 shows the corrosion process model of the coated medium-Mn steel in a marine atmosphere in this work. There are micro-defects in the AlN film, such as pores, pinholes, and cracks [15], and the corrosive liquid will permeate into these defects (Fig. 9a). After being exposed to the corrosion environment for a sufficient duration, AlN is hydrolyzed, and it can cause micro-stress locally. Then, micro-cracks appear, and they become the channel (pitting core) of the corrosive liquid (Figure 9b).

In the third stage shown in Fig. 9c, the corrosion channel reaches the Al film. Al becomes the second layer of protection and pitting corrosion occurs. As the corrosion progresses, the corrosion pits gradually become larger and deeper. Then, the corrosion runs through Al, as shown in Fig. 9d, and corrosion occurs in the medium-Mn steel. During the subsequent process shown in Fig. 9e, Al corrodes as the anode, and the medium-Mn steel is protected partially.

After the Al film is completely corroded, Al near the border is enriched (Fig. 7b). Because of the confined space formed by the porous AlN, the matrix is partially protected. The content of Fe is significantly higher near the interface than on the surface of the sample (Fig. 7b). The deposition of Al/AlN film can also restrain the formation of Mn_xO_y , and the content of Mn_xO_y is significantly lower in the corrosion product (Fig. 2a and Fig. 2b).

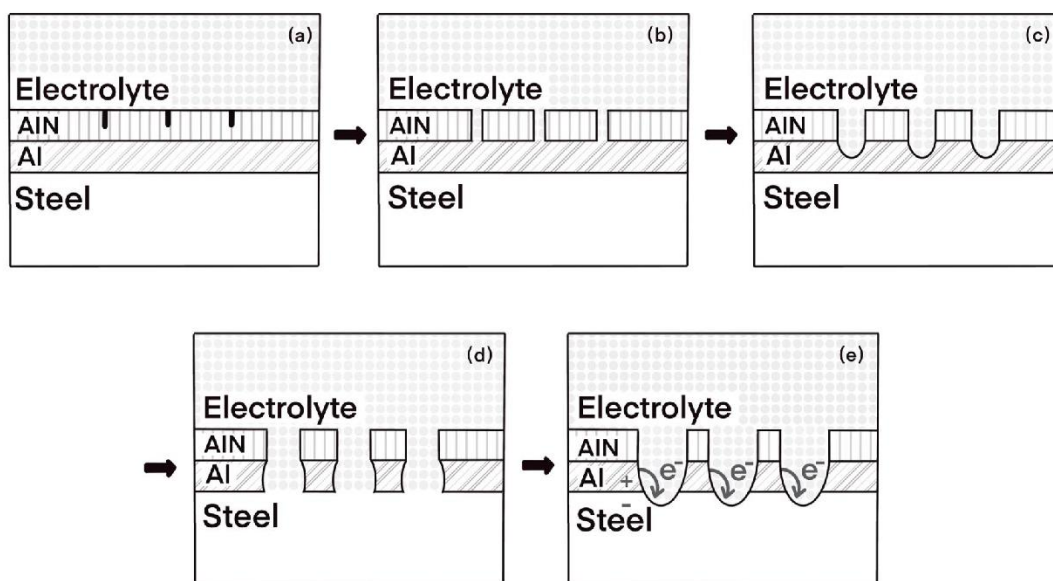


Figure 9. Corrosion process model of coated medium-Mn steel in the atmosphere of neutral salt spray

With the progress of corrosion, some γ -FeOOH transforms into α -FeOOH with a more stable structure. The relative confined space on the surface of the coated sample can promote the formation of α -FeOOH. Throughout the corrosion test in this work, the α/γ value of the coated sample is higher than that of the uncoated one, resulting in better corrosion resistance of the coated sample (Fig. 3). On the other hand, the hydrolysate AlN with a porous structure acts as a barrier to the corrosive liquid for the medium-Mn steel. As a result, the corrosion rate is significantly reduced, and the corrosion products are fewer than those of the uncoated medium-Mn steel.

In summary, the corrosion resistance of medium-Mn steel in a marine atmosphere is significantly improved by the deposition of Al/AlN film.

5. CONCLUSIONS

In this work, an Al/AlN film is successfully prepared and deposited on the surface of medium-Mn steel by DC magnetron sputtering. The deposition of Al/AlN film can promote the formation of α -FeOOH and increase the α/γ value in the rust layer of medium-Mn steel while restraining the formation of Mn_xO_y . The rust layer of the coated medium-Mn steel is thinner and more compact than that of the uncoated one, providing better protection for medium-Mn steel. Both Al and AlN films can provide sufficient protection to medium-Mn steel and reduce the corrosion rate of the sample. The deposition of Al/AlN film can significantly improve the corrosion resistance of medium-Mn steel.

ACKNOWLEDGEMENTS

Authors thank the foundation of Science and Technology research in Hebei Universities (ZD2018213), the Science and Technology Research and Development Projects of Handan City (19422111008-20), the National Natural Science Foundation of China (No. 51874114), and the Key Research Project of Higher Education in Hebei Province (ZD2021020) for the financial support of investigations.

References

1. J. Hu, L.X. Du, H. Liu, G.S. Sun, H. Xie, H.L. Yi and R.D.K. Misra, *Mater. Sci. Eng., A*, 647 (2015) 144.
2. H. Choi, S. Lee, J. Lee, F. Barlet and B.C.D. Cooman, *Mater. Sci. Eng., A*, 687 (2017) 200.
3. S.S. Li, P.Y. Wen, S.L. Li, W.W. Song, Y.D. Wang and H.W. Luo, *Acta Mater.*, 205 (2021) 116567.
4. M. Itagaki, R. Nozue, K. Watanabe, H. Katayama and K. Noda, *Corros. Sci.*, 46 (2004) 1301.
5. I. Diaz, H. Cano, D. Fuente, B. Chico, J.M. Vega and M. Morcillo, *Corros. Sci.*, 76 (2013) 348.
6. M. Kemp, A.V. Bennekoum and F.P.A. Robinson, *Mater. Sci. Eng., A*, 199 (1995) 183.
7. G.Q. Su, X.H. Gao, D.Z. Zhang, C.S. Cui, L.X. Du, C. Yu, J. Hu and Z.G. Liu, *Corrosion*, 73 (2017) 1367.
8. T.T. Xia, L.F. Zeng, X.H. Zhang, J. Liu, W.L. Zhang, T.X. Liang and B. Yang, *Surf. Coat. Technol.*, 363 (2019) 390.
9. Y.F. Zhang, Q.C. Du, T.G. Lin, S.W. Tang and J. Hu, *Coatings*, 11 (2021) 1399.
10. M. Wu, L. Pan, H. Duan, C. Wan, T. Yang, M. Gao and S. Yu, *Coatings*, 11 (2021) 1457.
11. J.L. Li, S.D. Mao, K.F. Sun, X.M. Li and Z.L. Song, *J. Magn. Magn. Mater.*, 321 (2009) 3799.

12. B. Wang, S.H. Wei, L. Guo, Y.J. Wang, Y. Liang, B. Xu, F.S. Pan, A.T. Tang and X.H. Chen, *Ceram. Int.*, 43 (2017) 10991.
13. A. Vahl, S. Veziroglu, B. Henkel, T. Strunskus, O. Polonsky, O.C. Aktas and F. Faupel, *Materials*, 12 (2019) 2840.
14. W.L. Xie, Y.M. Zhao, B. Liao, P. Pang, D.S. Wu and S. Zhang, *Vacuum*, 188 (2021) 110146.
15. H. Altun and S. Sen, *Surf. Coat. Technol.*, 197 (2004) 193.
16. P. Roberge, *Handbook of Corrosion Engineering*, McGraw-Hill, (2000) New York, USA.
17. Z.Q. Wang, Z.Y. Zhou, W.C. Xu, D. Yang, Y. Xu, L.H. Yang, J. Ren, Y.T. Li and Y.L. Huang, *Environ. Sci. Pollut. Res.*, 28 (2021) 54403.
18. M.H. Sun, C.W. Du, Z.Y. Liu, C. Liu, X.G. Li and Y.M. Wu, *Corros. Sci.*, 186 (2021) 109427.
19. Y.W. Liu, M.R. Liu, X. Lu and Z.Y. Wang, *Mater. Chem. Phys.*, 277 (2022) 124962.
20. Q. Feng, H. Kanoh and K. Ooi, *J. Mater. Chem.*, 9 (2002) 319.
21. Z. Liu, X.T. Lian, T.S. Liu, Y.D. Yang, J.N. Zhu and H. Dong, *Mater. Corros.*, 71 (2019) 258.
22. Y.H. Qian, C.H. Ma, D. Niu, J.J. Xu and M.S. Li, *Corros. Sci.*, 74 (2013) 424.
23. G.Q. Su, X.H. Gao, M.S. Huo, H.B. Xie, L.X. Du, J.Z. Xu and Z.Y. Jiang, *Constr. Build. Mater.*, 261 (2020) 119908.

© 2022 The Authors. Published by ESG (www.electrochemsci.org). This article is an open access article distributed under the terms and conditions of the Creative Commons Attribution license (<http://creativecommons.org/licenses/by/4.0/>).